Chaos-assisted adiabatic passage

Kyungsun Na and L. E. Reichl
Center for Studies in Statistical Mechanics and Complex Systems, The University of Texas at Austin, Austin, Texas 78712, USA

(Received 24 March 2004; revised manuscript received 2 July 2004; published 9 December 2004)

We study the exact dynamics underlying stimulated Raman adiabatic passage (STIRAP) for a particle in a multilevel anharmonic system (the infinite square well) driven by two sequential laser pulses, each with constant carrier frequency. In phase space regions where the laser pulses create chaos, the particle can be transferred coherently into energy states different from those predicted by traditional STIRAP. It appears that a transition to chaos can provide an additional tool to control the outcome of STIRAP.

DOI: 10.1103/PhysRevA.70.063405 PACS number(s): 32.80.Bx, 32.80.Qk, 05.45.−a

I. INTRODUCTION

Laser radiation provides a means to control intramolecular processes in a robust manner because of a conservation law that comes into play when monochromatic radiation interacts with nonlinear systems. The origin of this conservation law is the discrete time-translation invariance of laser-driven systems. For radiation interacting with molecular systems, this conservation law gives rise to stable electron-photon (phonon-photon, roton-photon) structures described by conserved eigenstates (the Floquet states) of the driven system. Floquet states are exact eigenstates of periodically driven systems [1–3]. Their reality can be seen in recent atom-optic experiments [4–6,3], where millions of sodium [5] or cesium atoms [4], interacting with a time-modulated standing wave of light, underwent large coherent periodic oscillations in momentum in a multiphoton process. These coherent oscillations were subsequently found to be due to the interference of only two or three Floquet eigenstates whose phase space structure was determined by an underlying chaotic sea induced by the interaction between the atoms and light [6]. In this paper, we wish to show that similar mechanisms are important when laser pulses interact with intramolecular forces. We will focus on the exact dynamics underlying stimulated Raman adiabatic passage (STIRAP) for laser pulses interacting with a simple model of intramolecular dynamics.

STIRAP has become an important tool for coherently controlling and changing the vibration and electronic states of entire molecular populations with close to 100% efficiency. STIRAP involves the application of short laser pulses with carefully chosen carrier frequencies to a molecular system for the purpose of exciting the molecules in a controlled manner. This technique causes a coherent change in the entire molecular population between molecular states. Traditional models of STIRAP generally view the molecular target as a simplified multilevel system. Indeed, traditional STIRAP focuses on three carefully chosen vibration and/or electronic levels. There are no studies, that we know of, that look at the effect on STIRAP of the actual nonlinear dynamics that occurs when the laser pulses interact with a molecular system. However, we know that laser pulses can induce chaos and this can strongly affect the response of the molecule to the laser field. In addition the internal dynamics of the molecule may itself be exhibiting the manifestations of chaos and simple pictures of the molecular level structure are likely not valid. Understanding this dynamics is very important for extending STIRAP to wider ranges of molecules

In this paper we study the *exact dynamics* underlying STIRAP for a model system that contains the essential features of low-energy vibration states, or rotational states, of a diatomic molecule driven by two laser pulses. We will find, for example, that in phase space regions where the laser pulses create chaos, the molecule can be transferred coherently into energy states very different from those predicted by traditional STIRAP. It appears that a transition to chaos may provide an additional tool to control the outcome of these processes in molecular systems.

STIRAP was first proposed by Hioe and co-workers [7,8] and later confirmed in an experiment involving population transfer between vibration-rotation states of sodium dimers [9,10]. There are several variations to STIRAP which generally is described as a process involving three particular energy levels, E_1, E_2, and E_3, of a collection of atoms or molecules of interest. All atoms or molecules are initially in the lowest-energy state E_1. Two laser pulses then impinge sequentially on the system in order to make a transition toward the target state E_3. In the "ladder" version of STIRAP the target state E_3 is the highest state in energy and in the "Λ" version of the STIRAP the intermediate state E_2 is the highest state in energy. The first laser pulse couples E_2 and E_3 which contain no population, and the second laser pulse then couples E_1 and E_2. As a result of these processes, the entire atomic or molecular population is transferred coherently into the target state without populating the intermediate state after the laser pulses have passed [11–17].

As mentioned above, conventional STIRAP analyzes an atomic or molecular system in terms of three carefully chosen energy levels of the unperturbed system. However, complications arise in real applications since these systems are composed of multiple states due to the rotational, vibration, and electronic levels of the unperturbed system. Extension of STIRAP to multilevel systems has been discussed by a number of authors, generally in terms of simplified models using the rotating-wave approximation and three or more laser pulses [18–29]. Alternatively, Raman-chirped adiabatic passage schemes [27–29], in which the frequency of the incident laser pulse is continuously changed, have also been proposed

to allow the system to climb through a sequence of molecular energy levels.

In this paper we take a different approach to the problem. We consider the *exact dynamics* that takes place when the two laser pulses impinge on a multilevel system. Instead of isolating a certain number of levels of interest and analyzing the process in terms of the rotating-wave approximation, we will let the full multilevel dynamics evolve and allow the system to tell us how many levels we must keep to accurately describe the atomic or molecular dynamics when a radiation field is present. Unlike the previous studies which utilize more than two pulses in multilevel systems, we only apply two pulses and allow as many levels as dictated by the dynamics participate in the process. One way to see how many levels must be kept is to look at the underlying classical phase space of the system of interest. The laser field, when interacting with nonlinear intramolecular dynamics will induce nonlinear resonances and chaos in localized regions of the phase space. Those structures in the classical phase space which have a size greater than Planck's constant determine the structure of the Floquet eigenstates of the system, and thereby have a direct influence on the STIRAP process.

The model we use to study the effect of chaos on STIRAP in a multilevel system is that of a particle in an infinite square-well potential [30,31]. The infinite square-well potential is an anharmonic potential of the form x^{2n} in the limit $n\to\infty$. It can give some insight into the behavior of low-lying vibration states, or rotation states, of molecular systems in the presence of sequential laser pulses. An approximate version of the square-well potential we consider here could also be constructed in an atom-optics experiment [6] or in semiconductor heterostructures. The dynamics of a particle in an infinite square-well potential is also interesting because the laser pulses can cause the low-energy particle states to undergo a transition to chaos [32,33]. For the case of monochromatic laser fields, this transition to chaos is accompanied by a plateau of high-harmonic radiation whose cutoff is determined by the width in energy of the chaotic sea induced by the laser field [32].

In the sections below, we describe the behavior of a particle in an infinite square-well potential which is driven by two sequential laser pulses whose carrier frequencies are monochromatic and chosen to couple specific unperturbed energy levels of the particle in the square-well potential. We will find that for the case when the pulse amplitudes vary slowly in time so that the adiabatic theorem [34] is satisfied, the dynamics can be described in terms "snapshots" of the underlying classical phase space at selected times as the laser pulses pass through the system. In Sec. II, we describe the classical dynamics that results from the laser pulses. In Sec. III, we discuss how we will describe the quantum dynamics for the driven system. In Sec. IV we introduce Floquet theory. In Secs. V–VII we show that a dynamics quite different from that of the traditional STIRAP ladder model can occur in multilevel systems due to the presence of chaos, even for fairly weak pulse amplitudes. Finally in Sec. VIII we make some concluding remarks.

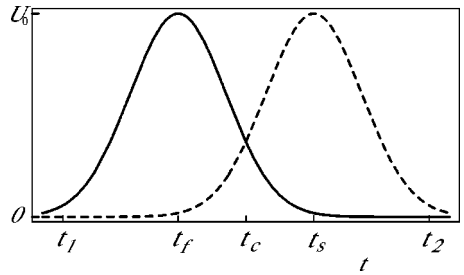

FIG. 1. Schematic diagram for the two pulses. The first pulse connecting levels $|E_2\rangle$ and $|E_3\rangle$ is shown as a solid line. The second pulse connecting levels $|E_1\rangle$ and $|E_2\rangle$ is shown as a dotted line. They have maximum strength U_0 at times $t=t_f$ and $t=t_s$, respectively. The whole pulse sequence takes a time $t=t_{tot}$ to complete. In the figure, $t_1=1/20t_{tot}$, $t_c=1/2t_{tot}$, and $t_2=19/20t_{tot}$.

II. CLASSICAL DYNAMICS

The model system for this study is a particle located in an infinite square well potential with spatial width $2a$. The potential energy has the form $V(\tilde{x})=0$ for $|\tilde{x}|<a$ and $V(\tilde{x})=\infty$ for $|\tilde{x}|\geqslant a$, where $\tilde{x}$ is the position of the particle. The classical Hamiltonian which describes the dynamics of a particle of mass m moving in the potential well and driven by two sequential pulses of monochromatic radiation is given by

$$\tilde{H}=\frac{\tilde{p}^2}{2m}+\tilde{U}_f(\tilde{t})\tilde{x}\cos(\tilde{\omega}_f\tilde{t})+\tilde{U}_s(\tilde{t})\tilde{x}\cos(\tilde{\omega}_s\tilde{t}) \quad \text{for } |\tilde{x}|<a, \tag{1}$$

where $\tilde{p}$ is the momentum of the particle, $\tilde{t}$ is the time, and $\tilde{\omega}_f$ and $\tilde{\omega}_s$ are the carrier frequencies of the first and second pulses, respectively. The amplitude of the first [second] pulse at time $\tilde{t}$ is $\tilde{U}_f(\tilde{t})$ $[\tilde{U}_s(\tilde{t})]$. If we rescale parameters using $\tilde{x}=xa$, $\tilde{p}=p\hbar/a$, $\tilde{U}_0=U_0\hbar^2/2ma^2$, $\tilde{t}=2ma^2t/\hbar$, $\tilde{H}=H\hbar^2/2ma^2$, and $\tilde{\omega}_{f,s}=\omega_{f,s}\hbar/2ma^2$, where $\hbar$ is Planck's constant, then the Hamiltonian is

$$H=p^2+U_f(t)x\cos(\omega_f t)+U_s(t)x\cos(\omega_s t) \quad \text{for } |x|<1, \tag{2}$$

and all parameters are dimensionless. The energy has been rescaled in units of $\hbar^2/2ma$ in order to make comparisons with the corresponding quantum system in subsequent sections.

The amplitudes $U_f(t)$ and $U_s(t)$ have Gaussian shape of the form

$$U_f(t)=U_0\exp[-\beta(t-t_f)^2], \quad U_s(t)=U_0\exp[-\beta(t-t_s)^2], \tag{3}$$

where $t_f<t_s$. We can control the duration of each pulse by adjusting the parameter β and we can control the amount of overlap of the two pulses by changing t_f and t_s. For simplicity, we assume that the maximum amplitude U_0 and width β of the two pulses are the same. A schematic picture of the variation in time of the amplitudes of the two pulses is displayed in Fig. 1. The first pulse is turned on and drives the particle in the square well and then, with an appropriate delay time, the second pulse is turned on. The whole pulse

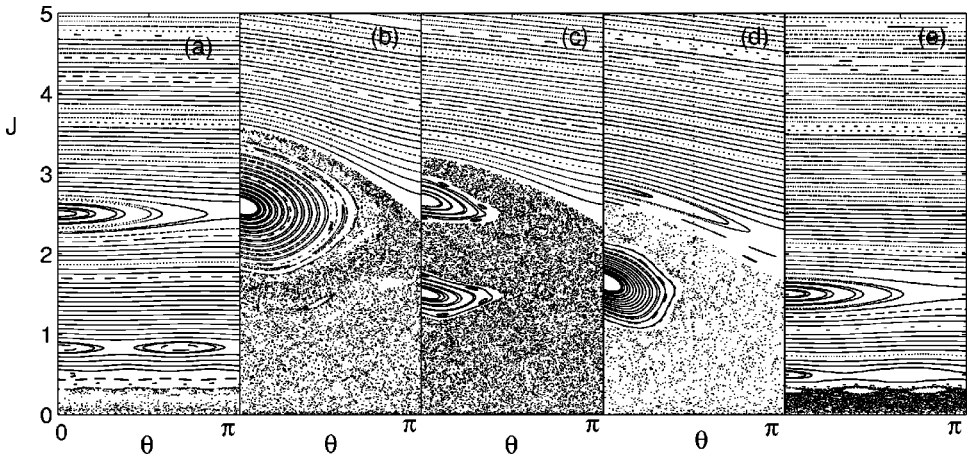

FIG. 2. Strobe plots of the action-angle variables (J,θ) for the infinite square-well system with pulse amplitudes $U_0=3.0$ and frequencies $\omega_f=5\omega_0$ and $\omega_s=3\omega_0$. Strobe plots are shown at times (a) $t_{fix}=t_1$, (b) $t_{fix}=t_f$, (c) $t_{fix}=t_c$, (d) $t_{fix}=t_s$, and (e) $t_{fix}=t_2$. For each plot $0\leqslant\theta\leqslant\pi$. The three largest primary resonances $\nu=1$, 2, and 3, due to the first pulse are located at $J=2.5$, 0.83, and 0.5. The three largest primary resonances $\nu=1$, 2, and 3, due to the second pulse are located at $J=1.5$, 0.5, and 0.3.

sequence ends at the total pulse duration time $t=t_{tot}$. For the purpose of marking time intervals in our subsequent discussion, we choose times $t_1=\frac{1}{20}t_{tot}$, $t_c=\frac{1}{2}t_{tot}$, and $t_2=\frac{19}{20}t_{tot}$.

We will be interested in how the classical phase space behaves in the *adiabatic limit* where the pulses are turned on and off very slowly relative to certain intrinsic time scales in the system, such as the periods of the carrier frequencies. In this limit the amplitudes $U_f(t)$ and $U_s(t)$ remain essentially constant during time intervals where the cosine terms oscillate many times. We can get an idea of the structure of the phase space by plotting a Poincaré surface of section of the phase space for fixed pulse amplitudes [3]. Thus we also consider the Hamiltonian

$$H=p^2+U_f(t_{fix})x\cos(\omega_f t)+U_s(t_{fix})x\cos(\omega_s t)\quad\text{for } |x|<1, \tag{4}$$

where the amplitudes are set to constants by choosing their value at some fixed time $t=t_{fix}$. The Hamiltonian in Eq. (4) is time periodic and we can view the behavior of the phase space using the Poincaré surfaces of section [3]. The Poincaré surfaces of section for time-periodic Hamiltonians are strobe plots of p and x—i.e., plots of p and x each time the Hamiltonian goes through one complete oscillation in time.

We can perform a canonical transformation to action-angle variables (J,θ) defined as $J=2|p|/\pi$ and $\theta=\pm\pi(x+1)/2$. The Hamiltonian then has the form

$$H=\frac{\pi^2J^2}{4}-\frac{4U_f(t_{fix})}{\pi^2}\sum_{\nu=-\infty}^{\infty}\frac{1}{(2\nu-1)^2}\cos[(2\nu-1)\theta-\omega_f t]$$
$$-\frac{4U_s(t_{fix})}{\pi^2}\sum_{\nu=-\infty}^{\infty}\frac{1}{(2\nu-1)^2}\cos[(2\nu-1)\theta-\omega_s t]$$
$$\text{for } 0\leqslant\theta\leqslant\pi. \tag{5}$$

An infinite number of nonlinear resonances are produced in the classical phase space by the external fields. The *primary resonances* are located at $J=J_\nu\equiv 2\omega_{f,s}/[(2\nu-1)\pi^2]$. As ν increases, the energy at which higher order primary resonances are located decreases.

In Fig. 2, we show strobe plots of the classical phase space for the case with $U_0=3.0$. The commensurability of these frequencies will allow us to use Floquet theory when we analyze the quantum system. We choose the pulse carrier frequencies to be $\omega_f=3\pi^2/4$ and $\omega_s=5\pi^2/4$. For the frequencies we have chosen, the period of the Hamiltonian is $T_0=8/\pi$. For the five cases shown in Figs. 2(a)–2(e), we fix the amplitude of the pulses by setting (a) $U_{f,s}(t_{fix})\equiv U_{f,s}(t_1)$, (b) $U_{f,s}(t_{fix})\equiv U_{f,s}(t_f)$, (c) $U_{f,s}(t_{fix})\equiv U_{f,s}(t_c)$, (d) $U_{f,s}(t_{fix})\equiv U_{f,s}(t_s)$, and (e) $U_{f,s}(t_{fix})\equiv U_{f,s}(t_2)$, respectively. For each of these choices of amplitude U_f and U_s, we show strobe plots of the classical phase space, allowing the time dependence of the cosine waves to vary. The three largest primary resonances $(\nu=1,2,3)$ induced by the first pulse are located at $J=2.5$, $J=0.83$, and $J=0.5$, respectively. The three largest primary resonances $(\nu=1,2,3)$ induced by the second pulse are located at $J=1.5$, $J=0.5$, and $J=0.3$, respectively. In Fig. 2(a), with $U_f(t_1)=0.1667$ and $U_s(t_1)=0.000\,003$, the primary resonances induced by the first pulse are dominant. In Fig. 2(e), with $U_f(t_2)=0.000\,003$ and $U_s(t_2)=0.1667$, the primary resonances induced by the second pulse are dominant. In all cases, the first primary resonance $(\nu=1)$ is located at the highest energy and the higher-order primary resonances are located at decreasing energy as ν increases. As a result, this system will always have a chaotic region at low energy due to the overlap of higher-order resonances. For energies above the region of influence of the $\nu=1$ primary of the first pulse, the phase space is dominated by Kolmogorov-Arnold-Moser (KAM) tori.

In Fig. 2(c), where $t_{fix}=t_c=\frac{1}{2}t_{tot}$, the primary $\nu=1$ resonances due to the two pulses have equal amplitude and are clearly visible at $J=2.5$ and $J=1.5$. For this case the pulse amplitudes are $U_f(t_c)=U_s(t_c)=1.103$. All the higher-order primary resonances have been destroyed and a large chaotic sea has formed at low energy.

Figure 2(b) shows the classical phase space at time $t_{fix}=t_f$ when the first pulse reaches its maximum amplitude with $U_f(t_f)=3.0$ and $U_s(t_f)=0.055$. The region of phase space about the primary $\nu=1$ resonance due to the first pulse is very distorted by the resonance. Detailed calculation shows that there are small higher-order (nonprimary) resonance islands between $J=3$ and $J=4$. Figure 2(d) shows the classical phase space at time $t_{fix}=t_s$ when the second pulse has reached its maximum amplitude with $U_f(t_s)=0.055$ and $U_s(t_s)=3.0$. The primary $\nu=1$ resonance due to the first pulse

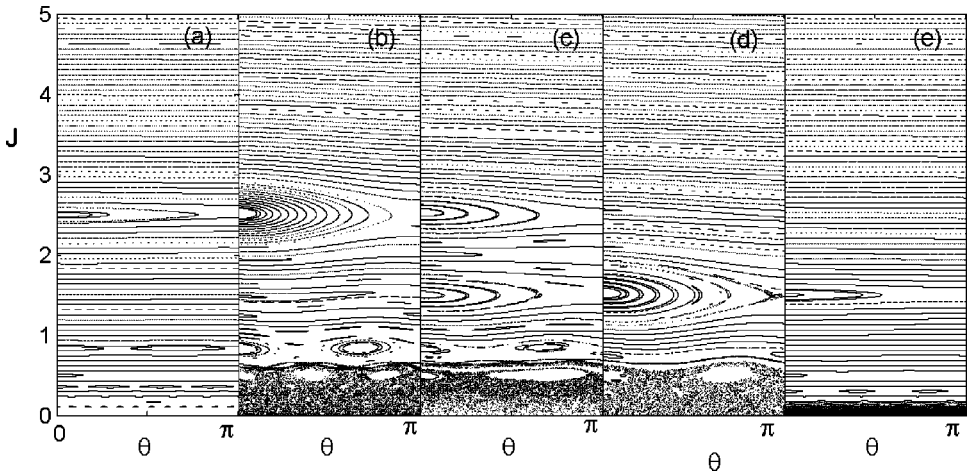

FIG. 3. Strobe plots of the action-angle variables (J,θ) for the infinite square-well system with pulse amplitudes $U_0=0.5$ and frequencies $\omega_f=5\omega_0$ and $\omega_s=3\omega_0$, respectively. Strobe plots are shown at times (a) $t_{fix}=t_1$, (b) $t_{fix}=t_f$, (c) $t_{fix}=t_c$, (d) $t_{fix}=t_s$, and (e) $t_{fix}=t_2$. For each plot $0\leqslant\theta\leqslant\pi$.

is very small and its region of influence does not extend very high in energy.

It is interesting to compare the classical phase space for $U_0=3.0$ with a case when the maximum pulse amplitude is $U_0=0.5$. In Fig. 3, we show the strobe plots of the classical phase space at the same times $t_{fix}=t_1$, t_f, t_c, t_s, and t_2 as in Fig. 2 but with $U_0=0.5$. More island structures survive with this relatively weak value of pulse amplitude than in Fig. 2. The invariant surfaces between the two $\nu=1$ primary resonances are distorted and higher order non-primary resonance islands can be seen even when the pulse amplitudes have reached their maximum values.

III. QUANTUM SYSTEM

The Schrödinger equation for the driven square-well system described in Sec. II can be written (in dimensionless units)

$$i\frac{\partial}{\partial t}\langle x|\psi(t)\rangle=\left(-\frac{\partial^2}{\partial x^2}+U_f(t)x\cos(\omega_f t)+U_s(t)x\cos(\omega_s t)\right)\times\langle x|\psi(t)\rangle, \tag{6}$$

where the momentum operator is given by $\hat{p}=-i\partial/\partial x$. In order to satisfy the boundary condition at $x=\pm1$, the wave function should satisfy $\psi(x=\pm1,t)=\langle x=\pm1|\psi(t)\rangle=0$ for all times t.

For the case of a quantum particle in an infinite square well, when $U_{f,s}=0$ (no driving force), the energy is conserved and we have a complete set of orthonormal energy eigenstates which can be used as basis states to describe the dynamics of the driven system. For the unperturbed system, the energy eigenvalues are $E_n=n^2\pi^2/4$ and the orthonormal energy eigenstates are $\langle x|E_n\rangle=\phi_n(x)=\sin[n\pi(x-1)/2]$. The dipole matrix elements in this basis are $x_{n,n'}=\langle E_n|\hat{x}|E_{n'}\rangle$ where

$$x_{n,n'}=\begin{cases}0 & [n+n'] \ \text{(modulo 2)}=0,\\ \dfrac{16nn'}{\pi^2(n^2-n'^2)^2} & [n+n'] \ \text{(modulo 2)}=1.\end{cases} \tag{7}$$

Note that integer values of J $(J=n)$ in the classical Hamiltonian correspond to the allowed quantized states of the quantum system. This simplifies comparison between the classical and quantum systems.

We can expand the wave function $|\psi(t)\rangle$, in the unperturbed energy basis, so $|\psi(t)\rangle=\Sigma_n c_n(t)|E_n\rangle$. Then we can rewrite the Schrödinger equation in the form

$$\frac{dc_n(t)}{dt}=-iE_nc_n(t)+i[U_f(t)\cos(\omega_f t)+U_s(t)\cos(\omega_s t)]\sum_{n'}x_{n,n'}c_{n'}(t), \tag{8}$$

where $c_n(t)=\langle E_n|\psi(t)\rangle$ is the probability amplitude to find the system in the nth energy level at time t. We will generally assume that at time $t=0$ the system is in the state $|\psi(0)\rangle=|E_1\rangle$. We will then find the state $|\psi(+\infty)\rangle$ after the two pulses have been turned on and off.

IV. FLOQUET STATES

Once we fix the amplitudes $U_f(t=t_{fix})=U_f(t_{fix})$ and $U_s(t=t_{fix})=U_s(t_{fix})$, the Hamiltonian becomes time periodic and the Schrödinger equation takes the form

$$i\frac{\partial}{\partial t}\langle x|\psi(t)\rangle=\left(-\frac{\partial^2}{\partial x^2}+U_f(t_{fix})x\cos(\omega_f t)+U_s(t_{fix})x\cos(\omega_s t)\right)\times\langle x|\psi(t)\rangle. \tag{9}$$

For such systems, the energy is not conserved. However, if the carrier frequencies of the pulses are commensurate, so $\omega_f/\omega_s=n_f/n_s$, where n_f and n_s are integers, then the Hamiltonian is invariant under a discrete time translation $H(t)=H(t+T_0)$, where the period T_0 of the Hamiltonian is

$$T_0=\pi\left(\frac{n_f}{\omega_f}+\frac{n_s}{\omega_s}\right). \tag{10}$$

For such systems, Floquet eigenstates $|\phi_\alpha(t)\rangle$ [which have period T_0 so $|\phi_\alpha(t+T_0)\rangle=|\phi_\alpha(t)\rangle$] form a complete orthonormal basis which determines the dynamics. Furthermore, the Floquet eigenphases Ω_α are conserved quantities [1–3].

We can obtain an eigenvalue equation relating Ω_α and $|\phi_\alpha(t)\rangle$. Consider the case when the system is in the αth

Floquet eigenstate so that $|\psi(t)\rangle = e^{-i\Omega_\alpha t}|\phi_\alpha(t)\rangle$. Then substitution into Eq. (9) yields the eigenvalue equation

$$\left(\hat{H}(t) - i\frac{\partial}{\partial t}\right)|\phi_\alpha(t)\rangle = \Omega_\alpha|\phi_\alpha(t)\rangle, \tag{11}$$

where $\hat{H}_F(t) \equiv \hat{H}(t) - i\partial/\partial t$ is the Floquet Hamiltonian.

More generally, when the system is in the state $|\psi(0)\rangle$ at time $t=0$, the state of the system at time t can be written

$$|\psi(t)\rangle = \sum_\alpha A_\alpha e^{-i\Omega_\alpha t}|\phi_\alpha(t)\rangle = \sum_\alpha \langle\phi_\alpha(0)|\psi(0)\rangle e^{-i\Omega_\alpha t}|\phi_\alpha(t)\rangle. \tag{12}$$

The state of the system at time $t=T_0$ takes on an especially simple form

$$|\psi(T_0)\rangle = \hat{U}_F(T_0)|\psi(0)\rangle = \sum_\alpha e^{-i\Omega_\alpha T_0}|\phi_\alpha(0)\rangle\langle\phi_\alpha(0)|\psi(0)\rangle, \tag{13}$$

where we have used the fact that $|\phi_\alpha(T_0)\rangle = |\phi_\alpha(0)\rangle$. The Floquet evolution operator $\hat{U}_F(T_0)$, can now be defined:

$$\hat{U}_F(T_0) = \sum_\alpha e^{-i\Omega_\alpha T_0}|\phi_\alpha(0)\rangle\langle\phi_\alpha(0)|. \tag{14}$$

We can compute matrix elements of the Floquet evolution operator in the basis of unperturbed energy eigenstates. Then the (n,n')th matrix element of the resulting Floquet matrix is given by

$$\begin{aligned} U_{n,n'}(T_0) &= \langle E_n|\hat{U}_F(T_0)|E_{n'}\rangle \\ &= \sum_\alpha e^{-i\Omega_\alpha T_0}\langle E_n|\phi_\alpha(0)\rangle\langle\phi_\alpha(0)|E_{n'}\rangle. \end{aligned} \tag{15}$$

The αth eigenvalue of the Floquet matrix $U_{n,n'}(T_0)$ is $\exp(-i\Omega_\alpha T_0)$, and the αth eigenvector in the unperturbed energy basis is given by a column matrix composed of matrix elements, $\langle E_n|\phi_\alpha(0)\rangle$, where $n=1,\ldots,\infty$. The eigenvalues Ω_α can be obtained from $\exp(-i\Omega_\alpha T_0)$, but only with modulus ω_0. We refer to the eigenvalues Ω_α obtained from the Floquet matrix as *eigenphases*.

For the system we consider here, the Floquet matrix has a natural truncation which is determined by the nonlinear dynamics of the system. Classically, the driven square-well system has a region of mixed phase space bounded at high energies by KAM tori. For the cases we will consider here, where the initial state $|\psi(0)\rangle$ is the unperturbed energy level $|\psi(0)\rangle = |E_1\rangle$, the state $|\psi(0)\rangle$ can never penetrate very far into the high-energy KAM region. This provides a natural truncation of the size of the Floquet matrix and we need to include only enough unperturbed basis states $|E_n\rangle$ to cover adequately the region of mixed phase space. Each column of the Floquet matrix can be constructed by solving the time-dependent Schrödinger equation for one period T_0 with the system initially in one of the unperturbed energy eigenstates. This integration is performed using each of the unperturbed energy eigenstates as an initial state until all the columns of the Floquet matrix have been computed. Floquet eigenphases and eigenstates are obtained by numerically diagonalizing the Floquet matrix [3].

Husimi distributions allow us to visualize the distribution of probability of the Floquet eigenstates in the underlying classical phase space [35]. Physically they describe the location of the particle in the presence of the radiation field and provide important information about the actual dynamics taking place in the system. The Husimi distribution for a Floquet eigenstate $|\phi_\alpha\rangle$ is defined as $H(x_0,p_0) = |\langle\phi_\alpha|x_0,p_0\rangle|^2$, where the state $|x_0,p_0\rangle$ is a coherent state that can be represented in the position basis as [32]

$$\langle x|x_0,p_0\rangle = \left(\frac{1}{\sigma^2\pi}\right)^{1/4}\exp\left(-\frac{(x-x_0)^2}{\sigma^2} + \frac{ip_0(x-x_0)}{\hbar}\right). \tag{16}$$

The coherent state is a minimum uncertainty wave packet and has a parameter σ that determines the relative dispersion in both position and momentum space.

In the subsequent sections, we will consider three different choices for carrier frequencies of the pairs of pulses which drive the system. For case I, the first pulse connects levels $n=2$ and $n=3$ and the second pulse connects levels $n=1$ and $n=2$. This is the traditional model for the STIRAP ladder process [11]. However, as distinct from the usual discussion of STIRAP we will deal with the exact dynamics of the system. We will take account of the fact that we have a multilevel system that can undergo a transition to chaos. We will examine the effect of the full nonlinear dynamics on this system. For case II, the first pulse connects levels $n=4$ and $n=5$ and the second pulse connects levels $n=1$ and $n=4$. This is again a ladder process. For this case the underlying chaotic dynamics will have a surprising effect on the transition probabilities. Finally, for case III, we consider a Λ process in which the first pulse connects levels $n=3$ and $n=4$ and the second pulse connects levels $n=1$ and $n=4$. In all cases, we consider the exact dynamics of the driven system.

V. CASE I: FIRST PULSE 2→3, SECOND PULSE 1→2

In this section, we examine the dynamics of the driven square-well system when two pulses are applied such that the first pulse connects levels $n=2$ and $n=3$ and the second pulse then connects the levels $n=1$ and $n=2$. We first determine the behavior of Floquet eigenstates at fixed times $t=t_{fix}$ during which the pulses drive the system. The distribution of probability in the Floquet eigenstates is sensitive to structures in the classical phase space which are larger than Planck's constant. We then compare the prediction of Floquet theory to the actual behavior of the system in the nonadiabatic and adiabatic regimes.

A. Behavior of Floquet eigenstates

The first pulse has carrier frequency $\omega_f = (E_3 - E_2) = 5\pi^2/4$ and the second pulse has carrier frequency $\omega_s = (E_2 - E_1) = 3\pi^2/4$. These frequencies are commensurate since

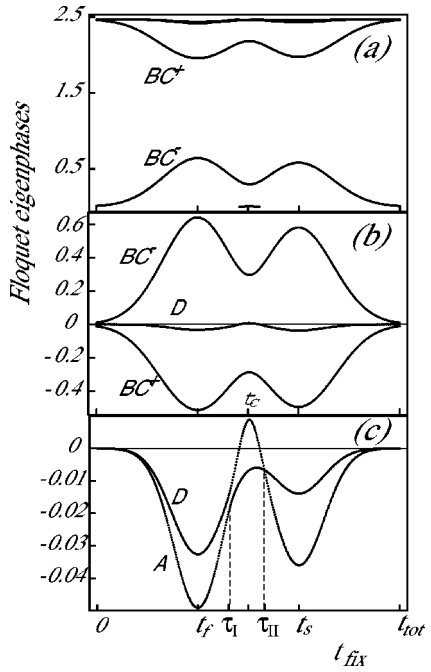

FIG. 4. Floquet eigenphases, for the system with maximum pulse strength $U_0=3.0$ and frequencies $\omega_f=5\omega_0$ and $\omega_s=3\omega_0$, are plotted over the entire interval $0\leqslant t_{fix}\leqslant t_{tot}$. (a) Floquet eigenphases for four Floquet states A, BC^+, BC^-, and D plotted mod $\omega_0=\pi^2/4$. (b) Floquet eigenphase curves for the Floquet states D, BC^+, and BC^-. The three-level-wide avoided crossing at $t_{fix}=t_c$ is clear. (c) Floquet eigenphase curves for the Floquet states A and D. The sharp avoided crossing at $t_{fix}=\tau_I$ and the crossing at $t_{fix}=\tau_{II}$ are clearly seen.

$\omega_f/\omega_s=5/3$. From Eq. (10), the period of the Hamiltonian is $T_0=8/\pi$ and the *Floquet frequency* is $\omega_0=2\pi/T_0=\pi^2/4$. Thus, $\omega_f=5\omega_0$ and $\omega_s=3\omega_0$. We set $U_0=3.0$.

The dynamics of this system tells us that we only need to keep five unperturbed energy eigenstates as a basis to form the Floquet matrix. This can be seen from Fig. 2 where we show the underlying classical phase space at selected values of t_{fix} during the time that the pulses are on. For $J>5$, the classical phase space is dominated by KAM tori with almost constant values of J and the unperturbed energy states are very weakly coupled by the dynamics for $n>5$. Thus, to describe the quantum behavior of this system, it is sufficient to construct a 5×5 Floquet matrix with the five basis states $|E_1\rangle,\ldots,|E_5\rangle$. We find that only four of the five eigenstates of the Floquet matrix are actively involved in the dynamics. Their eigenphases Ω_α are plotted modulo $\omega_0=\pi^2/4$ in Fig. 4(a). Two of these Floquet eigenphases are almost degenerate over the time interval that the pulses act and are not distinguishable on the scale shown in Fig. 4(a). For $t_{fix}=0$, the four Floquet eigenphases are approximately degenerate modulo ω_0.

We can follow each Floquet eigenstate during the entire process by computing the eigenstates for a sequence of values of t_{fix} over the interval $0\leqslant t_{fix}\leqslant t_{tot}$. For closely spaced values of t_{fix}, Floquet eigenstates at different times belonging to different eigenphases will be orthogonal. This provides a means of following the evolution of each eigenstate as a function of t_{fix}. As we will see, the Floquet eigenstates can change structure when avoided crossings occur between Floquet eigenphases. To keep track of the changes that occur in the Floquet eigenstates, we will give each eigenstate a unique alphabetical label determined by its dominant dependence on unperturbed energy states at time $t_{fix}=0$. We find that at $t_{fix}=0$ the Floquet eigenstates have the following structure and we give them the following labels:

$$A=|\phi_1\rangle=|E_1\rangle,\quad D=|\phi_4\rangle=|E_4\rangle,\quad E=|\phi_5\rangle=|E_5\rangle,$$

$$BC^+=|\phi_2\rangle=\frac{1}{\sqrt{2}}(|E_2\rangle+|E_3\rangle),\tag{17}$$

$$BC^-=|\phi_3\rangle=\frac{1}{\sqrt{2}}(|E_2\rangle-|E_3\rangle).$$

The traditional STIRAP ladder process assumes that the molecule or atom in question can be approximated by a three level system and causes a coherent population shift of the atom from level 1 to level 3. We find that the traditional STIRAP ladder process occurs in our system for $U_0<0.1$. For amplitudes $U_0<0.1$, state $D=|\phi_4\rangle$ does not participate in the dynamics at all. The Floquet eigenvalue curve for Ω_4, plotted as a function of t_{fix}, crosses that for Ω_1 in two places but does not undergo any avoided crossings. The state $D=|\phi_4\rangle$ remains predominantly dependent on $|E_4\rangle$ during the entire process. For traditional STIRAP, curve D in Fig. 4(b) is replaced by state A and the only avoided crossing that occurs is the three-way avoided crossing at $t_{fix}=t_c$ between states A, BC^+, and BC^-. State A, which is predominantly composed of the state $|E_1\rangle$ before the multiple avoided crossing at $t=t_c$, becomes predominately dependent on state $|E_3\rangle$ after the multiple avoided crossing, having interchanged its "1" character with the "3" character of states BC^+ and BC^- at the avoided crossing. Thus, at the end of the process state A would be composed predominately of level $n=3$ and the states BC^+ and BC^- would be predominately of superpositions of levels $n=1$ and $n=2$.

Once the amplitude U_0 becomes greater than $U_0=0.1$, something different happens due to the avoided crossing shown in Fig. 4(c). For $U_0<0.1$ the Floquet eigenphases for states A and D in Fig. 4(c) *cross* at time $t_{fix}=\tau_I\approx\frac{10}{23}t_{tot}$ just before $t_{fix}=t_c$. For $U_0>0.1$ the Floquet eigenphases for states A and D in Fig. 4(c) *avoid crossing* at time $t_{fix}=\tau_I$. Before time $t_{fix}=\tau_I$ Floquet state A is predominately composed of level $n=1$ and Floquet state D is predominately composed of level $n=4$. After the avoided crossing at time $t_{fix}=\tau_I$ the states have changed their character and Floquet state A is composed predominately of level $n=4$ and Floquet state D is composed predominately of level $n=1$. Because of the avoided crossing at $t_{fix}=\tau_I$, the entire population gets shifted from level $n=1$ to level $n=4$ *before* the traditional STIRAP ladder process can take place. The traditional STIRAP ladder process now occurs among *unpopulated* states. It is interesting to note that the Floquet states A and D *cross* at time $t_{fix}=\tau_{II}\approx13/23t_{tot}$. A symmetry that was broken earlier appears to have been restored. These transitions are clearly seen in Fig. 5 where we show the level compositions of the

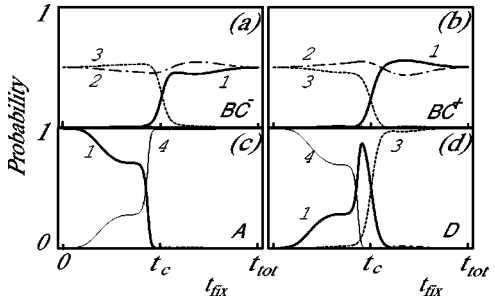

FIG. 5. Probability distribution $|\langle E_n|\phi_\alpha\rangle|^2$ of the unperturbed energy levels $|E_n\rangle$ which compose each of the Floquet eigenstates (a) BC^- (b) BC^+, (c) A, and (d) D, plotted over the entire interval $0 \leqslant t_{fix} \leqslant t_{tot}$ for pulse amplitude $U_0=3.0$ and frequencies $\omega_f=5\omega_0$ and $\omega_s=3\omega_0$. The probability curve for level $|E_n\rangle$ is labeled with level quantum number n.

four participating Floquet states A, BC^+, BC^-, and D as a function of t_{fix}.

B. Population transfer

Let us now determine the exact behavior of the system, when the pulses are applied, by solving the Schrödinger equation in (8). We will assume that at time $t=0$ the system is in state $|\psi(0)\rangle=|E_1\rangle$. As we will see, the actual dynamics of this system is determined by the length of time during which the pulses are allowed to act. The pulse duration time necessary to achieve adiabatic behavior of the system is determined largely by the avoided crossings in the Floquet eigenphases. At isolated avoided crossings, involving only two eigenstates, the states involved interchange their character.

Avoided crossings of Floquet eigenphases occur as the classical phase space becomes chaotic, and a symmetry has been broken in that local region of the phase space. The probability P_{LZ} that a transition occurs between the two Floquet eigenstates involved in an *isolated* avoided crossing can be computed from a formula obtained independently by Landau [36] and Zener [37]. For our system, the Landau-Zener probability is given by

$$P_{LZ} = \exp\left(-\frac{\pi(\delta\epsilon)^2}{2\gamma}\right), \tag{18}$$

where $\delta\epsilon$ is the eigenphase spacing at the avoided crossing and γ is the rate of change of the Floquet eigenphases with respect to time t_{fix} in the neighborhood of the avoided crossing.

We have computed the Landau-Zener probability P_{LZ} for the isolated sharp avoided crossing at time $t_{fix}=\tau_I$ shown in Fig. 4(c). The Landau-Zener probability depends on t_{tot}. The larger t_{tot}, the more "stretched out" the horizontal axis in Fig. 4(c) will be relative to the vertical axis. We have obtained the following results by analyzing Fig. 4(c) for different values of t_{tot}. For $t_{tot}=120$, $\delta\epsilon=0.005$ and $\gamma=0.001\,875$, giving a Landau-Zener probability $P_{LZ}=0.979\,270$. For $t_{tot}=21\,000$, $\delta\epsilon=0.0063$ and $\gamma=0.000\,013\,76$, giving a Landau-Zener probability $P_{LZ}=0.0108$. For $t_{tot}=270\,000$, $\delta\epsilon=0.0030$ and $\gamma=1.2\times10^{-7}$, giving a Landau-Zener probability $P_{LZ}\approx 0$. The first case is not in the adiabatic regime, but the second two cases are in the adiabatic regime because the probability of a transition is negligible.

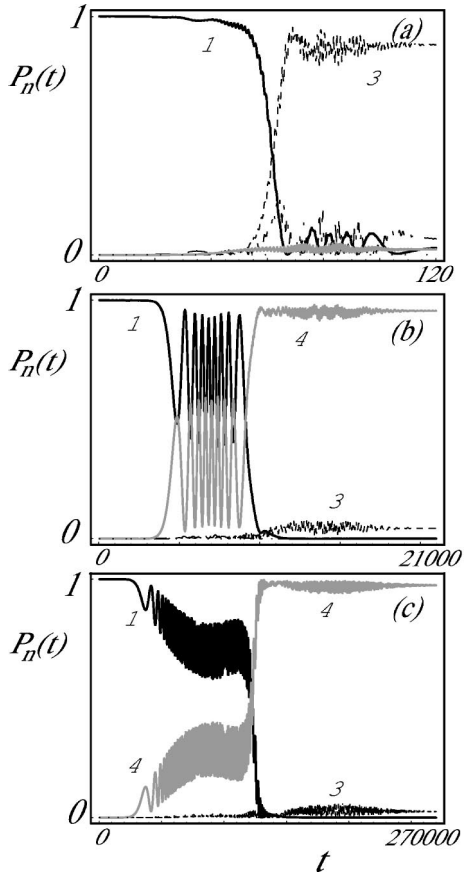

FIG. 6. The probability $P_n(t)=|\langle E_n|\psi(t)\rangle|^2$ to find the system in the unperturbed level $|E_n\rangle$ for the system prepared in initial state $|\psi(0)\rangle=|E_1\rangle$ with maximum pulse strength $U_0=3.0$ and frequencies $\omega_f=5\omega_0$ and $\omega_s=3\omega_0$. The total pulse duration times are (a) $t_{\rm tot}=120$, (b) $t_{\rm tot}=21\,000$, and (c) $t_{\rm tot}=270\,000$. The numbers attached to each curve show the components of the transition probability in terms of the unperturbed energy eigenstate basis. Case (a) is not in the adiabatic regime. Cases (b) and (c) are within the adiabatic regime and basically reproduce the structure of the single Floquet eigenstate A in Fig. 5(c).

In Fig. 6, we show the probability $P_n(t)=|\langle E_n|\psi(t)\rangle|^2$ (for the four levels $n=1$, 2, 3, 4) to find the system in the nth unperturbed level at time t for the three cases $t_{tot}=120$, $t_{tot}=21\,000$, and $t_{tot}=270\,000$. These results are obtained by directly solving the Schrödinger equation (8). In all cases we start the system in the initial state $|\psi(0)\rangle=|E_1\rangle$ with maximum pulse strength $U_0=3.0$. In Fig. 6(a), where there is a large Landau-Zener probability for the system to jump from Floquet state A to Floquet state D, the system comes out of the sharp avoided crossing at $t_{fix}=\tau_I$ still predominately in the level $|E_1\rangle$ and the traditional STIRAP ladder process can then occur at $t=t_c$. As the pulses are turned on and off, the system transitions from level $|E_1\rangle$ to level $|E_3\rangle$. In Figs. 6(b) and 6(c), the Landau-Zener probability is essentially zero and no transition occurs at the sharp avoided crossing at

$t_{fix}=\tau_I$. The system comes out of the sharp avoided crossing in level $|E_4\rangle$. As the laser pulses are turned on and off the system transitions from the initial state $|\psi(0)\rangle=|E_1\rangle$ to the final state $|\psi(+\infty)\rangle=|E_4\rangle$. Note that both Figs. 6(b) and 6(c) follow almost exactly the behavior of the Floquet state *A* shown in Fig. 5(c). This is an indication that we are in the adiabatic regime in Figs. 6(b) and 6(c).

The very large oscillations in the probability in Figs. 6(b) and 6(c) have been explained by Berry [38] in terms of a sequence of "superadiabatic bases." He shows that the decrease in the amplitude of these oscillations as we increase t_{tot} is a sign that we are moving further into the adiabatic regime. The frequencies of the oscillations in Figs. 6(b) and 6(c) appear to be determined by the difference in Floquet eigenphases of the two Floquet states involved in the sharp avoided crossing. For example, at $t_{fix}=t_f$ the period of the oscillation is $T_{osc}\approx 400$. The difference in the Floquet eigenphases is $|\Delta\Omega|=|\Omega_1-\Omega_4|\approx 0.016$. Thus, $T_{osc}=2\pi/|\Delta\Omega|=393$. Similarly, at $t_{fix}=(\tau_I-t_f)/2$, $T_{osc}\approx 600$. The difference in the Floquet eigenphases is $|\Delta\Omega|=|\Omega_1-\Omega_4|\approx 0.011$. Thus, $T_{osc}=2\pi/|\Delta\Omega|=571$. The observed oscillation periods are the same for both Fig. 6(b) and Fig. 6(c).

VI. CASE II: FIRST PULSE 4→5, SECOND PULSE 1→4

We now turn on pulses with higher carrier frequencies in order to examine more closely the relation between the quantum transitions and their relation to the underlying classical dynamics. We first apply a pulse whose carrier frequency is $\omega_f=(E_5-E_4)=9\pi^2/4$. We then apply a second pulse whose carrier frequency is $\omega_s=(E_4-E_1)=15\pi^2/4$. The two frequencies are commensurate since $\omega_f/\omega_s=3/5$. From Eq. (10), the periods of the Hamiltonian and Floquet frequency are again $T_0=8/\pi$ and $\omega_0=\pi^2/4$, respectively. Thus, $\omega_f=9\omega_0$ and $\omega_s=15\omega_0$. We will consider the case when the maximum amplitude of both pulses is $U_0=13.0$. For these frequencies and amplitudes, we find that we can induce a transition of the entire population from level $|E_1\rangle$ to level $|E_{10}\rangle$. Below we describe how this happens.

Classical phase space plots for times $t_{fix}=t_f$, $t_{fix}=t_c$, $t_{fix}=\tau_{IV}=3/5t_{tot}$, and $t_{fix}=t_s$ are shown in Figs. 7(a)–7(d), respectively. The first primary resonance due to the first pulse is located at $J=4.5$ and the first primary resonance due to the second pulse is located at $J=7.5$. The frequency of the second pulse is chosen to connect levels $n=1$ and $n=4$. However, it also connects the levels $n=7$ and $n=8$ since $E_8-E_7=15\omega_0$. This is why the first primary resonance due to the second pulse lies at $J=7.5$. The states below $J=4.0$ are immersed in the chaotic sea formed by the higher-order primaries induced by the two pulses during most of the time that the one or the other of the pulses have a significant strength. Higher-order nonprimary resonance islands can be seen above $J=6.0$ during most of the pulse sequence. In Fig. 7(b) there is a chaotic sea which has formed throughout the region $J=0-9$. Also, during the last half of the pulse sequence, the KAM tori near $J=10$ are highly distorted due to the formation of the primary resonance at $J=7.5$. Thus, from classical phase space we see that it requires approximately

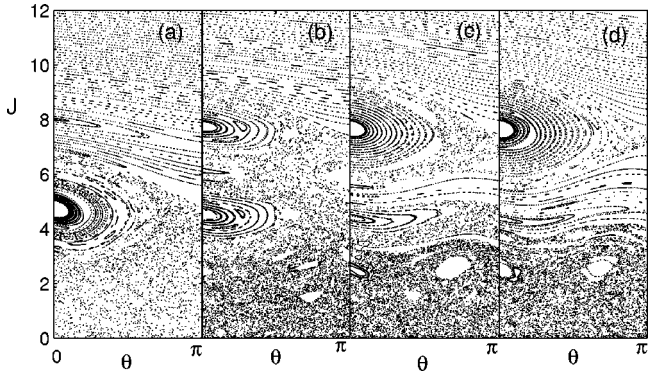

FIG. 7. Strobe plots of the action-angle variables (J,θ) for the infinite square-well system with pulse amplitudes $U_0=13.0$ and frequencies $\omega_f=9\omega_0$ and $\omega_s=15\omega_0$, respectively. Strobe plots are shown at times (a) $t_{fix}=t_f$, (b) $t_{fix}=t_c$, (c) $t_{fix}=\tau_{IV}=3/5t_{\mathrm{tot}}$, and (d) $t_{fix}=t_s$. The first primary resonance from the first pulse is located at $J=4.5$ and the first primary resonance from the second pulse is located at $J=7.5$.

12 square-well energy eigenstates to accurately describe the dynamics of this system.

The Floquet matrix that we use to describe the quantum dynamics is a 12×12 matrix. However, we find that only ten Floquet eigenstates are directly involved in the dynamics. To keep track of these ten Floquet eigenstates, we will give each state a unique alphabetical label determined by their dominant dependence on unperturbed energy states at time $t_{fix}=0$. We find that at $t_{fix}=0$ the Floquet eigenstates have the following structure and we give them the following labels:

$$A=|\phi_1\rangle=|E_1\rangle,\ B=|\phi_2\rangle=|E_2\rangle,\ C=|\phi_3\rangle=|E_3\rangle,$$
$$F=|\phi_6\rangle=|E_6\rangle,$$

$$DE^+=|\phi_4\rangle=\frac{1}{\sqrt{2}}(|E_4\rangle+|E_5\rangle),\ DE^-=|\phi_5\rangle=\frac{1}{\sqrt{2}}(|E_4\rangle-|E_5\rangle),$$

$$G=|\phi_7\rangle=|E_7\rangle,\ H=|\phi_8\rangle=|E_8\rangle,\ I=|\phi_9\rangle=|E_9\rangle,$$
$$J=|\phi_{10}\rangle=|E_{10}\rangle. \tag{19}$$

The Floquet eigenphases corresponding to these ten Floquet eigenstates are plotted modulo ω_0 in Fig. 8. A number of avoided crossings occur between the eigenphases during the time the pulses act on the system. There are four avoided crossings that largely determine the dynamics. There is a multiple wide avoided crossing at $t_{fix}=t_c=\frac{1}{2}t_{tot}$ which involves the seven states *B*, *C*, $DE^{\pm}$, *F*, *H*, and *I*. There is a sharp avoided crossing at $t_{fix}=\tau_{III}\approx\frac{3}{8}t_{tot}$ that involves the states *B* and *G*. There is a three-state wide avoided crossing at $t_{fix}=\tau_{IV}\approx\frac{3}{5}t_{tot}$ that involves states *A*, *B*, and *H*. There is a sharp avoided crossing at $t_{fix}=\tau_V\approx\frac{2}{3}t_{tot}$ which involves the states *A* and *J*.

In Fig. 9(a) we plot the eigenphases of the seven Floquet states *B*, *C*, $DE^{\pm}$, *F*, *H*, and *I* involved in the multiple avoided crossing at $t_{fix}=t_c=\frac{1}{2}t_{tot}$. These states have support in the unperturbed square-well levels E_3, E_4, E_5, E_6, E_7, E_8, and E_9. In Fig. 9(b) we show a magnification of the very sharp

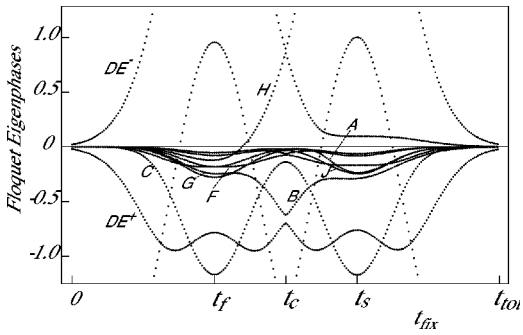

FIG. 8. The ten Floquet eigenphases, plotted modulo ω_0, which determine the dynamics for pulse strength $U_0=13.0$ and frequencies $\omega_f=9\omega_0$ and $\omega_s=15\omega_0$. The curves are identified following the classification scheme in Eq. (19).

avoided crossing between states DE^- and H at $t_{fix}=t_c=\frac{1}{2}t_{tot}$. The effect of these avoided crossings can be seen in the dependence of the Floquet eigenstates on the square-well states $|E_n\rangle$. Plots of Floquet eigenstates B, H, and G are shown in Fig. 10 and plots of Floquet eigenstates $DE^{\pm}$, C, and F are shown in Fig. 11. There is a complicated interchange of levels occurring. As shown in [33], at such multiple avoided crossings, the Floquet eigenstates emerge with very different probability distributions than the entering states. Thus, multiple avoided crossings behave differently from isolated pairs of avoided crossings where the states simply interchange character. Multiple avoided crossings provide a mechanism for the spread of the manifestations of chaos in quantum systems [33].

It is useful to note that there is an isolated avoided crossing at $t_{fix}=\tau_{III}$ that causes states B and G to switch from B

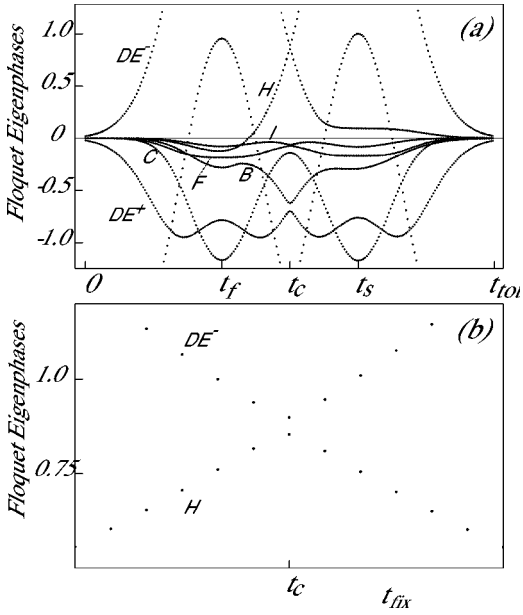

FIG. 9. (a) The seven Floquet eigenphases, plotted modulo ω_0, which are involved in the multiple avoided crossing at $t_{fix}=t_c=\frac{1}{2}t_{\rm tot}$ for pulse strength $U_0=13.0$ and frequencies $\omega_f=9\omega_0$ and $\omega_s=15\omega_0$. The curves are identified following the classification scheme in Eq. (19). (b) A magnification of the very sharp avoided crossing between Floquet states DE^- and H at $t_{fix}=t_c=\frac{1}{2}t_{\rm tot}$.

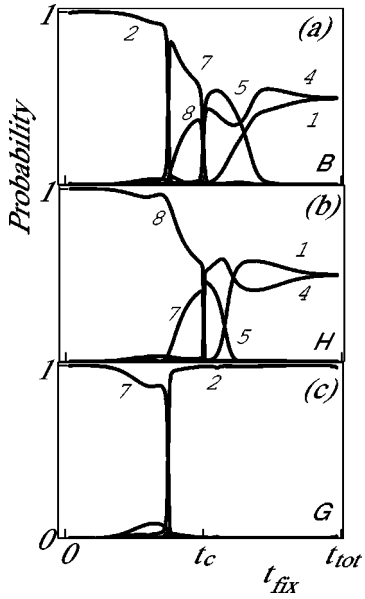

FIG. 10. Probability distribution $|\langle E_n|\phi_\alpha\rangle|^2$ of the unperturbed energy levels which compose each of the Floquet eigenstates (a) B, (b) H, and (c) G, plotted over the entire interval $0\leqslant t_{fix}\leqslant t_{\rm tot}$ for pulse strength $U_0=13.0$ and frequencies $\omega_f=9\omega_0$ and $\omega_s=15\omega_0$. The probability curve for level $|E_n\rangle$ is labeled with level quantum number n.

$\approx|E_2\rangle$ and $G\approx|E_7\rangle$, as they enter the avoided crossing at τ_{III}, to $B\approx|E_7\rangle$ and $G\approx|E_2\rangle$ as they leave. Thus state $B\approx|E_7\rangle$ as it enters the multiple avoided crossing at $t_{fix}=t_c=\frac{1}{2}t_{tot}$.

Let us now consider the transition that causes the population of the square well to undergo a coherent transition from level $|E_1\rangle$ to level $|E_{10}\rangle$. This can occur if the system evolves adiabatically and follows the behavior of Floquet state A. The level dependence of Floquet state A is shown in Fig. 12(a). It starts out in level $|E_1\rangle$ and then partially switches to level $|E_5\rangle$ at $t_{fix}=\tau_{IV}$ due to a three state avoided crossing between states A, B, and H, and finally at $t_{fix}=\tau_V$ it switches completely to level $|E_{10}\rangle$ due to a sharp avoided crossing between states A and J. The avoided crossings at times $t_{fix}=\tau_{IV}$ and $t_{fix}=\tau_V$ that cause these transitions are shown in Figs. 13(a) and 13(b), respectively.

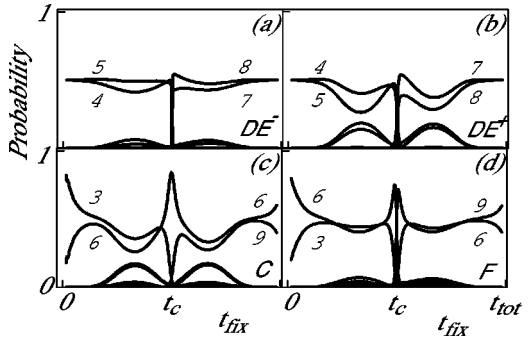

FIG. 11. Probability distribution $|\langle E_n|\phi_\alpha\rangle|^2$ of the unperturbed energy levels which compose each of the Floquet eigenstates (a) DE^-, (b) DE^+, (c) C, and (d) F plotted over the entire interval $0\leqslant t_{fix}\leqslant t_{\rm tot}$ for pulse strength $U_0=13.0$ and frequencies $\omega_f=9\omega_0$ and $\omega_s=15\omega_0$. The probability curve for level $|E_n\rangle$ is labeled with level quantum number n.

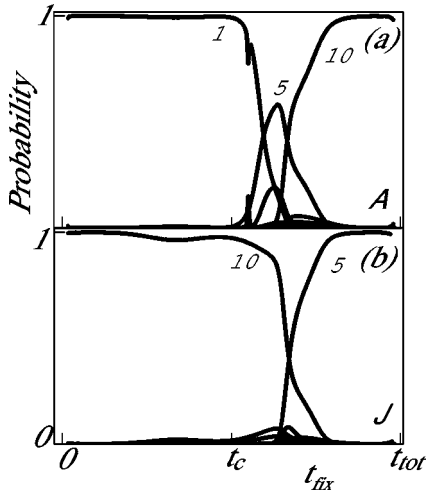

FIG. 12. Probability distribution $|\langle E_n|\phi_\alpha\rangle|^2$ of the unperturbed energy levels which compose each of the Floquet eigenstates (a) *A* and (b) *J*, plotted over the entire interval $0 \leq t_{fix} \leq t_{\mathrm{tot}}$ for pulse strength $U_0=13.0$ and frequencies $\omega_f=9\omega_0$ and $\omega_s=15\omega_0$. The probability curve for level $|E_n\rangle$ is labeled with level quantum number *n*.

In Fig. 14 we show a sequence of Husimi plots of the states *B*, *H*, *A*, and *J* as they go through the avoided crossings at $t_{fix}=\tau_{IV}$ and $t_{fix}=\tau_V$. The Husimi plots show the location of the quantum particle in phase space when the system is in a given eigenstate. The columns from left to right show the Floquet states *B*, *H*, *A*, and *J*. From top to bottom, the Husimi plot of each state is shown at times (a) $t_{fix}=t_f$, (b) $t_{fix}=t_c$, (c) $t_{fix}=\tau_{IV}$, (d) $t_{fix}=\tau_V$, and (e) $t_{fix}=t_2$. The sequence of events causing Floquet state *A* to undergo a transition from level $|E_1\rangle$ to level $|E_{10}\rangle$ can be seen clearly in these plots.

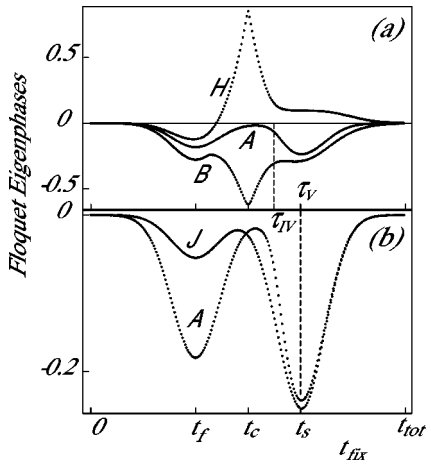

FIG. 13. (a) Magnification of the three Floquet eigenphases for eigenstates *A*, *B*, and *H* which are involved in the three-state avoided crossing at $t_{fix}=\tau_{IV}=3/5t_{\mathrm{tot}}$ for pulse strength $U_0=13.0$ and frequencies $\omega_f=9\omega_0$ and $\omega_s=15\omega_0$. The curves are identified following the classification scheme in Eq. (19). (b) Magnification of the sharp avoided crossing at $t_{fix}=\tau_V=2/3t_{\mathrm{tot}}$ for pulse strength $U_0=13.0$ and frequencies $\omega_f=9\omega_0$ and $\omega_s=15\omega_0$. Curves of eigenphases for Floquet eigenstates *A* and *J* are shown.

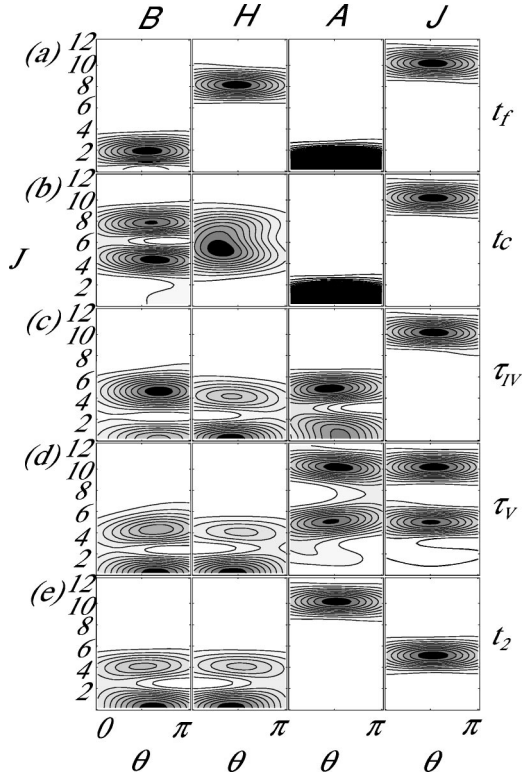

FIG. 14. Husimi plots for the Floquet states (a) *B*, (b) *H*, (c) *A*, and (d) *J* plotted in columns from left to right, respectively, for maximum pulse strength $U_0=13.0$ and frequencies $\omega_f=9\omega_0$ and $\omega_s=15\omega_0$. Each Floquet state (column) is shown (from top to bottom) at times (a) $t_{fix}=t_f$, (b) $t_{fix}=t_c$, (c) $t_{fix}=\tau_{IV}=3/5t_{\mathrm{tot}}$, (d) $t_{fix}=\tau_V=2/3t_{\mathrm{tot}}$, and (e) $t_{fix}=t_2$. The effect of the avoided crossings that enable Floquet state *A* to undergo a transition from level $|E_1\rangle$ to level $|E_{10}\rangle$ can be seen clearly.

Finally in Figs. 15(a) and 15(b), we plot the probability $P_n(t)=|\langle E_n|\psi(t)\rangle|^2$ (for the ten levels $n=1,\ldots,10$) to find the system in the *n*th unperturbed level at time *t* [Fig. 15(c) will be discussed in Sec. VII]. The system is prepared in initial state $|\psi(0)\rangle=|E_1\rangle$ with maximum pulse strength $U_0=13.0$. We obtain these plots by directly solving the Schrödinger equation (8). In Fig. 15(a) we show the results for the nonadiabatic case. We choose $t_{tot}=600$ which is a rapid evolution of the pulses. After the pulses have passed, the final state of the system is $|\psi(+\infty)\rangle=|E_5\rangle$. The adiabatic case is shown in Fig. 15(b). We now choose $t_{tot}=6000$. The probabilities now closely follow the behavior of the single Floquet eigenstate *A* as can be seen in Fig. 12(a). After the pulses have passed, the final state of the system is $|\psi(+\infty)\rangle=|E_{10}\rangle$. This transition dynamics is determined by the structure of the avoided crossings in the Floquet eigenphase curves and by the phase space structure of the Floquet eigenstates at the avoided crossing.

The phase space structure of the Floquet eigenstates (see the Husimi plots) is determined by structures in the underlying classical phase space which are greater than Planck's constant. The transition from $|\psi(0)\rangle=|E_1\rangle$ to $|\psi(\infty)\rangle=|E_{10}\rangle$ occurs because at the time of the transition the classical phase space is connected by a chaotic sea from $J=1$ to *J*

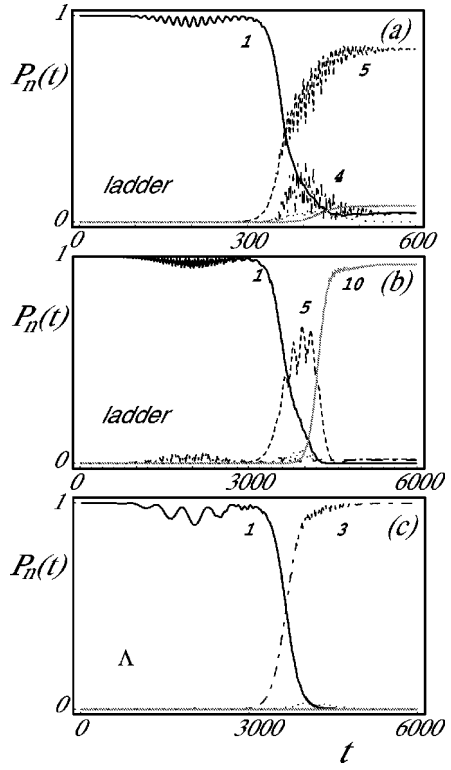

FIG. 15. The probability $|\langle E_n|\psi(t)\rangle|^2$ to find the system in the unperturbed level $|E_n\rangle$ for the system prepared in initial state $|\psi(0)\rangle=|E_1\rangle$ with maximum pulse strength $U_0=13.0$ for the ladder processes in (a) and (b) and for the Λ process (c). For the ladder process, the frequencies of both pulses are $\omega_f=9\omega_0$ and $\omega_s=15\omega_0$ and (a) $t_{\rm tot}=600$ and (b) $t_{\rm tot}=6000$. For the Λ process, the frequencies of both pulses are $\omega_f=7\omega_0$ and $\omega_s=15\omega_0$ and (c) $t_{\rm tot}=6000$. The numbers attached to each curve show the components of the transition probability in terms of the unperturbed energy levels.

=9 and a strongly distorted KAM region at $J=10$ which allows the quantum state to tunnel into the phase space region around $J=10$. This can be seen from the Husimi plot for the state A at time $t_{fix}=\frac{13}{20}t_{tot}$ which is shown in Fig. 16. The unperturbed levels $n=1$, $n=5$, and $n=10$ are connected via the chaotic sea around the two $\nu=1$ primary resonances which exist at the time $t_{fix}=\frac{13}{20}t_{tot}$.

VII. CASE III: FIRST PULSE 3→4, SECOND PULSE 1→4

The final case we consider is a Λ process in which the system is driven by pulses with carrier frequencies $\omega_f=(E_4-E_3)=7\pi^2/4$ and $\omega_s=(E_4-E_1)=15\pi^2/4$. These frequencies are commensurate and the period of the Hamiltonian and the Floquet frequency are again $T_0=8/\pi$ and $\omega_0=\pi^2/4$, respectively. To stay as close to case II parameters as possible, we chose pulse amplitudes $U_0=13.0$. Although this case looks similar to case II, we will find quite different results.

In the adiabatic limit, the transition $|E_1\rangle\rightarrow|E_3\rangle$ occurs, as shown in Fig. 15(c), which is very different from case II. We believe that the difference between these two processes is due to the difference in the phase space distribution of the resonances and chaos induced in the system by the laser

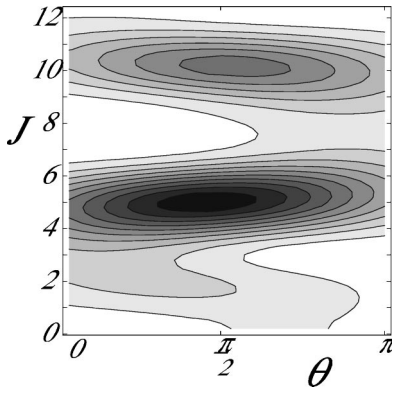

FIG. 16. Husimi plot for the Floquet state A for maximum pulse strength $U_0=13.0$ and frequencies $\omega_f=9\omega_0$ and $\omega_s=15\omega_0$ at time $t_{fix}=13/20t_{\rm tot}$, just before the avoided crossing at $t_{fix}=\tau_V$. This state covers the entire chaotic region of the underlying classical phase space from $J=1$ to $J=9$ and the highly distorted mixed region at $J=10$.

pulses. Strobe plots of the classical phase space for the Λ case for times $t_{fix}=t_f$, $t_{fix}=t_c$, $t_{fix}=\tau_{IV}=0.62t_{tot}$, and $t_{fix}=t_s$ are shown in Figs. 17(a)–17(d), respectively. The first primary resonance due to the first pulse is located at $J=3.5$ (rather than $J=4.5$ as is in case II) and the first primary resonance due to the second pulse is located at $J=7.5$ (the same as case II). For case II, a pathway is opened by a chaotic sea that allows a Floquet state to tunnel across the entire energy region (see Fig. 16) from $|E_1\rangle$ to $|E_{10}\rangle$ at the time of the avoided crossing. In the strobe plots of the classical phase space in Fig. 17 for case III, this pathway is blocked by KAM tori which do not allow the quantum system to tunnel out of the low energy region. We also find fewer avoided crossings in the plot of the Floquet eigenphases for this case.

VIII. CONCLUSION

We have found that sequential laser pulses, when applied to a particle in an anharmonic multilevel system, can induce

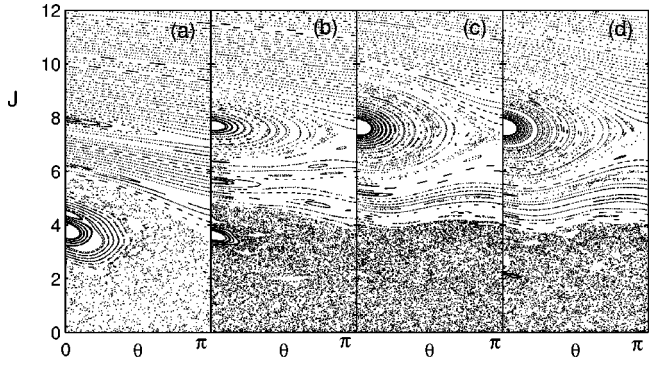

FIG. 17. Strobe plots of the action-angle variables (J,θ) for the infinite square-well system with pulse pulse amplitudes $U_0=13.0$ and frequencies $\omega_f=7\omega_0$ and $\omega_s=15\omega_0$, respectively. Strobe plots are shown at times (a) $t_{fix}=t_f$, (b) $t_{fix}=t_c$, (c) $t_{fix}=\tau_{IV}=0.60t_{\rm tot}$, and (d) $t_{fix}=t_s$. The first primary resonance from the first pulse is located at $J=3.5$ and the first primary resonance from the second pulse is located at $J=7.5$.

nonlinear resonances and a transition to chaos in the dynamics of the particle. The extent of the region influenced by resonances and chaos determines the number of unperturbed energy eigenstates that must be kept to form the basis used to construct the Floquet matrix and to determine the quantum dynamics.

When the pulses are applied in a manner which adiabatically changes the dynamics of the particle, this transition to chaos can be used to control the coherent transfer of the particle across the chaotic sea from a low-lying energy state to a highly excited energy state. Floquet theory provides an accurate means of describing the dynamical behavior of these driven systems in the adiabatic limit. The type of population transfer that is allowed depends on the nature of the Floquet eigenphase avoided crossings created by the underlying transition to chaos and the ability of the corresponding Floquet eigenstates to tunnel across vast regions of the phase space because of the induced chaos. In cases I and II, avoided crossings occurred between Floquet eigenstates which had spread throughout the available phase space, and a coherent flow of probability from the low-energy side to the high-energy side of the chaotic sea occurred. In case III, the path to the high-energy states around the resonance at $J=7.5$ appears to be blocked by KAM tori and the transition to the higher-energy states does not occur.

In molecular systems, the success of STIRAP will depend on the state of the dynamics of the unperturbed molecular system and on the changes in that dynamics induced by the laser pulses. Most molecular systems have regimes of internal chaos and the interplay of these regimes with the dynamics induced by the laser pulses is critical to understanding STIRAP in these system.

ACKNOWLEDGMENTS

The authors wish to thank the U.S. Navy Office of Naval Research (Grant No. N00014-03-1-0639) for support of this work and we wish to thank the Engineering Research Program of the Office of Basic Energy Sciences at the U.S. Department of Energy (Grant No. DE-FG03-94ER14465) for partial support of this work. L.E.R wishes to thank the Robert A. Welch Foundation (Grant No. F-1051) for partial support of this work. Both authors thank Dario Martinez for the useful discussions about Floquet theory. We also thank the University of Texas High Performance Computing Center for the use of its facilities.

[1] J. H. Shirley, Phys. Rev. **138**, B979 (1965).
[2] H. Sambe, Phys. Rev. A **7**, 2203 (1973).
[3] L. E. Reichl, *The Transition to Chaos: Conservative Classical Systems and Quantum Manifestations*, 2nd ed. (Springer-Verlag, Berlin, 2004).
[4] D. A. Steck, W. H. Oskay, and M. G. Raizen, Science **293**, 274 (2001); Phys. Rev. Lett. **88**, 120406 (2002).
[5] W. K. Hensinger, H. Haffner, A. Browaceys, N. R. Heckenberg, K. Helmerson, C. McKenzie, G. J. Milburn, W. D. Phillips, S. L. Rolston, H. Rubinsztein-Dunlop, and B. Upcrot, Nature (London) **412**, 52 (2001).
[6] R. Luter and L. E. Reichl, Phys. Rev. A **66**, 053615 (2002).
[7] F. T. Hioe, Phys. Lett. **99A**, 150 (1983).
[8] J. Oreg, F. T. Hioe, and J. H. Eberly, Phys. Rev. A **29**, 690 (1984).
[9] U. Gaubatz, P. Rudecki, M. Becker, S. Schiemann, M. Kulz, and K. Bermann, Chem. Phys. Lett. **149**, 463 (1988).
[10] U. Gaubatz, P. Rudecki, S. Schiemann, and K. Bermann, J. Chem. Phys. **92**, 5363 (1990).
[11] B. W. Shore, K. Bermann, and J. Oreg, Z. Phys. D: At., Mol. Clusters **23**, 33 (1992).
[12] B. W. Shore, *The Theory of Coherent Atomic Excitation* (Wiley, New York, 1990).
[13] M. V. Danileiko, V. I. Romanenko, and L. P. Yatsenko, Opt. Commun. **109**, 462 (1994).
[14] K. Bergmann, H. Theuer, and B. W. Shore, Rev. Mod. Phys. **70**, 1003 (1998).
[15] L. P. Yatsenko, B. W. Shore, K. Bergmann, and V. I. Romanenko, Eur. Phys. J. D **4**, 47 (1998).
[16] K. Drese and M. Holthaus, Eur. Phys. J. D **5**, 119 (1999).
[17] C. Y. Ye, V. A. Sautenkov, and M. O. Scully, Opt. Lett. **28**, 2213 (2003).
[18] B. W. Shore, K. Bergmann, J. Oreg, and S. Rosenwaks, Phys. Rev. A **44**, 7442 (1991).
[19] V. S. Malinovsky and D. J. Tannor, Phys. Rev. A **56**, 4929 (1997).
[20] F. T. Hioe and C. E. Carroll, Phys. Rev. A **37**, 3000 (1988).
[21] J. Oreg, K. Bergmann, B. W. Shore, and S. Rosenwaks, Phys. Rev. A **45**, 4888 (1992).
[22] A. V. Smith, J. Opt. Soc. Am. B **9**, 1543 (1992).
[23] Y. B. Band and P. S. Julienne, J. Chem. Phys. **95**, 5681 (1991).
[24] F. T. Hioe and C. E. Carroll, Phys. Lett. A **220**, 49 (1996).
[25] B. W. Shore, J. Martin, M. P. Fewell, and K. Bergmann, Phys. Rev. A **52**, 566 (1995).
[26] J. Martin, B. W. Shore, and K. Bergmann, Phys. Rev. A **52**, 583 (1995); **54**, 1556 (1996).
[27] B. Broers, H. B. van Linden van den Heuvell, and L. D. Noordam, Phys. Rev. Lett. **69**, 2062 (1992).
[28] S. Chelkowski and G. N. Gibson, Phys. Rev. A **52**, R3417 (1995).
[29] B. Y. Chang, I. R. Sola, V. S. Vladmir, S. Malinovsky, and J. Santamaris, Phys. Rev. A **64**, 033420 (2001).
[30] W. A. Lin and L. E. Reichl, Phys. Rev. A **40**, 1055 (1989).
[31] B. Galdrikian, B. Birnir, and M. Sherwin, Phys. Lett. A **203**, 319 (1995).
[32] W. Chism, T. Timberlake, and L. E. Reichl, Phys. Rev. E **58**, 1713 (1998).
[33] T. Timberlake and L. E. Reichl, Phys. Rev. A **59**, 2886 (1999).
[34] A. Messiah, *Quantum Mechanics* (North-Holland, Amsterdam, 1962), Vol. 2.
[35] K. Husimi, Proc. Phys. Math. Soc. Jpn. **22**, 248 (1940).
[36] L. D. Landau, Phys. Z. Sowjetunion **2**, 46 (1932).
[37] C. Zener, Proc. R. Soc. London, Ser. A **137**, 696 (1932).
[38] M. V. Berry, Proc. R. Soc. London, Ser. A **429**, 61 (1990).